Published in final edited form as:

*ACS Appl Mater Interfaces*. 2018 October 10; 10(40): 34792–34801. doi:10.1021/acsami.8b14128.

# Untemplated Resveratrol-Mediated Polydopamine Nanocapsule Formation

**Devang R. Amin**[1,2], **Cody J. Higginson**[1], **Angie B. Korpusik**[1], **Alyse R. Gonthier**[1], and **Phillip B. Messersmith**[1,3,*]

[1]Departments of Bioengineering and Materials Science and Engineering, University of California, Berkeley, 210 Hearst Mining Building, Berkeley, CA 94720 United States

[2]Department of Biomedical Engineering, Northwestern University, 2145 Sheridan Rd, Evanston, IL 60208 United States

[3]Materials Science Division, Lawrence Berkeley National Laboratory, Berkeley, CA 94720 United States

## Abstract

Nanocapsules can be designed for applications including drug delivery, catalysis, and biological imaging. The mussel-inspired material polydopamine is a promising shell layer for nanocapsules because of its free radical scavenging capacity, ability to react with a broad range of functional molecules, lack of toxicity, and biodegradability. Previous reports of PDA nanocapsule formation have relied on a templating approach. Herein, we report a template-free approach to polydopamine nanocapsule formation in the presence of resveratrol, a naturally occurring anti-inflammatory and antioxidant compound found in red wine and grapes. Synthesis of nanocapsules occurs spontaneously in an ethanolic resveratrol/dopamine·HCl solution at pH 8.5. UV-Vis absorbance spectroscopy and X-ray photoelectron spectroscopy indicate that resveratrol is incorporated into the nanocapsules. We also observed the formation of a soluble fluorescent dopamine-resveratrol adduct during synthesis which was identified by HPLC, UV-Vis spectroscopy, and ESI-MS. Using TEM and DLS, we studied the influence of solvent composition, dopamine concentration, and resveratrol:dopamine ratio on the nanocapsule diameter and shell thickness. The resulting nanocapsules have excellent free radical scavenging activity as measured by a DPPH radical scavenging assay. Our work provides a convenient pathway by which RV, and possibly other hydrophobic bioactive compounds, may be encapsulated within polydopamine nanocapsules.

## Graphical Abstract

*Corresponding author: philm@berkeley.edu; ph: 510-643-9631.

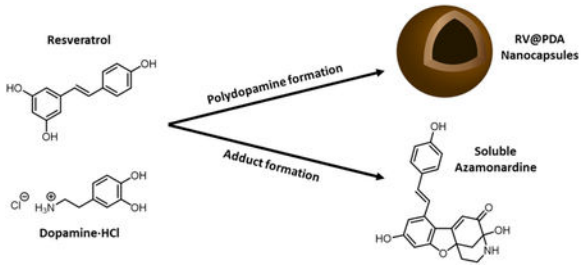


**Keywords**

dopamine; polydopamine; nanoparticle; resveratrol; capsule; nanocapsule

## 1. Introduction

Since the first report of mussel-inspired polydopamine (PDA) a little over a decade ago,[1] PDA has been widely explored for surface modification and as multifunctional coatings.[1-4] PDA coatings can be applied to a wide range of substrates by simple immersion in a mild alkaline solution of dopamine·HCl (DA). Under these conditions, DA autoxidation results in formation of dopamine-*o*-quinone and dihydroxyindole, which further react via poorly understood reactions culminating in the formation of a conformal coating of PDA on the substrate.[5-9] PDA serves as a convenient primer layer for further surface modification with organic and inorganic species through covalent bonding with amines and thiols, **π-π** stacking, hydrogen bonding, metal ion coordination, and electrostatic interactions.[1, 3, 10–12]

Colloidal particles such as gold nanoparticles[12-16], superparamagnetic iron oxide nanoclusters[17], mesoporous silica[18], carbon nanotubes[19-20], and PLGA nanoparticles[21] have similarly been coated with PDA primer layers for further modification with antibodies, peptides, chemotherapeutic drugs, aptamers, microRNAs, and metals. Sunoqrot et al. also observed that mPEG-PCL nanoparticles became muco-adhesive following PDA coating.[22] Additionally, colloidal particles of PDA have been prepared by autoxidation of dopamine under mild alkaline conditions for applications including free radical scavenging, fluorescent imaging, chemotherapeutic drug delivery, UV photoprotection, and near-infrared photothermal therapy.[23-29] PDA nanoparticles have been observed to be nontoxic in mammalian cell culture.[23-24, 26]

Nanocapsules (NCs), which have liquid cores surrounded by polymer or inorganic shells, have applications in drug delivery, vaccine delivery, catalysis, and biomedical imaging.[30-37] Existing literature reports on the formation of PDA micro- and nanocapsules[38-45] mainly rely upon “hard” or “soft” templates, which are first coated with PDA and then dissolved or etched away to yield a PDA capsule. In one study, Caruso and coworkers coated silica spheres with PDA by incubation with DA solution at pH 8.5 and then etched away the silica with hydrofluoric acid.[38] Using the silica templating approach, Caruso and coworkers were able to prepare fluorescent PDA capsules by subsequent $H_2O_2$ oxidation of the PDA.[41] Liu et al. deposited PDA on polystyrene beads and subsequently dissolved the beads with THF.[39] Shi and coworkers deposited PDA on a $CaCO_3$ mineral template and then dissolved the

mineral template to prepare PDA microcapsules for enzyme catalysis.[43-45] Soft-templated PDA capsules have also been prepared by creating an emulsion of dimethyldiethoxysilane droplets that were coated with PDA and then dissolved to yield 400 nm − 2.4 μm diameter PDA capsules could be loaded with CdSe/CdS quantum dots, magnetic $Fe_3O_4$ NPs, and hydrophobic drugs such as the chemotherapeutic drug doxorubicin.[40, 46-47]

Template-free approaches to the preparation of PDA capsules have the potential advantage of avoiding the need for aggressive treatments to remove the template.[38-41, 46] One template-free approach to PDA NC formation was recently developed by Ni et al,[42] who proposed that microphase separation of a THF-water solvent mixture formed microdroplets that were coated by PDA. However, this group did not report PDA capsules with diameters below 200 nm, or incorporation of cargo into the PDA capsules.

Here, we report the surprising discovery of spontaneous untemplated PDA nanocapsule formation from mixtures of dopamine and the bioactive molecule resveratrol (RV) without the use of toxic reagents. Naturally found in red wine and grapes, RV is a hydroxylated stilbene derivative that has reported anti-inflammatory, anti-cancer, anti-diabetic, cardioprotective and anti-aging effects. [48-50] We show that during PDA NC formation, a fraction of RV reacts with oxidized dopamine to form a soluble azamonardine fluorophore, whereas additional RV is incorporated into the PDA nanocapsules. Control over NC diameter and shell thickness was established by varying DA concentration and the RV:DA ratio. The antioxidant activity of RV@PDA nanocapsules was confirmed by a DPPH free radical scavenging assay, suggesting that the RV@PDA NCs may be useful for biological applications that require reduction of oxidative stress.

## 2. Experimental Section

### 2.1. Materials

Dopamine·HCl (DA, >98% purity) was purchased from Acros Organics (Thermo Fisher Scientific, Geel, Belgium). Resveratrol was purchased from Spectrum Chemical (New Brunswick, NJ, USA). 2,2-diphenyl-1-picrylhydrazyl (DPPH) was purchased from Sigma-Aldrich (St. Louis, MO, USA). Falcon® polypropylene conical tubes (50 mL, 30 × 115 mm style) were obtained from Corning (Corning, NY, USA). Ultrapure (UP) water was purified from deionized water with a Barnstead Ultrapure Water Purification System (Thermo Fisher Scientific, Waltham, MA, USA) to a resistivity of at least 18.0 MΩ cm. Koptec 200 proof ethanol was purchased from DeconLabs (King of Prussia, PA, USA). HPLC grade, submicron filtered acetonitrile was purchased from Fisher Scientific (Pittsburgh, PA, USA), and HPLC grade trifluoroacetic acid (TFA) was purchased from EMD Millipore (Millipore Sigma, Burlington, MA, USA).

### 2.2. Nanomaterial Synthesis and Purification

**RV@PDA and PDA Synthesis:** All solvents, buffers, and stock solutions were 0.22 μm filtered before use. In a typical synthesis, RV@PDA was prepared in solutions containing a 5:1 volume ratio of 10 mM bicine-buffered water and ethanol, 0.250 mg/mL DA, and 0.125 mg/mL resveratrol (0.5:1 RV:DA mass ratio). Ultrapure water (36.5 mL) and ethanol (7.83

mL) were first mixed in a 50 mL centrifuge tube. To this solution, resveratrol (RV) in ethanol (500 μL at 12.5 mg/mL) was added, and the tube was vortexed for several seconds. Then, DA in ultrapure water (1 mL at 12.5 mg/mL) was added to this solution. After vortexing several seconds, 100 mM bicine buffered water (pH 8.5, 4.17 mL) was added to the particle growth solution and vortexed again for several seconds. The growth solution was incubated with mild shaking for 24 h (setting #5 (~80 rpm) on a Stovall BDRAA115S Belly Dancer Shaker, Cole Parmer). After 24 h, the product was purified by centrifugation at 12,500 g for 40 minutes, rinsing once with ultrapure water. To evaluate the effect of solvent composition on NC diameter, the ratio of ethanol:water was adjusted as needed to achieve final solvent ratios of 2:1 – 12:1 of 10 mM bicine buffered water and ethanol.

PDA was synthesized and purified in the same manner as RV@PDA without adding resveratrol to the particle growth solution.

**Evaluation of the Effect of Delayed Buffer Addition:** In order to determine the effect of pre-incubating DA and RV before addition of buffer, the RV@PDA and PDA syntheses were performed as described above without the addition of buffer. Following mixing of DA, RV, water, and ethanol, the reaction mixture was incubated in a 50 mL centrifuge tube at either room temperature or at 60 °C for 24 h. Then, 4.17 mL of 100 mM bicine buffer at pH 8.5 was quickly added to the solution, which was then capped and vortexed for several seconds. The samples were then mixed rapidly as described above under non-turbulent conditions for 24 h at room temperature before purification by centrifugation at 12,500 g for 40 min, rinsing once with ultrapure water.

### 2.3. Dopamine-Resveratrol Adduct Purification and Characterization

**Purification of Dopamine-Resveratrol (DA-RV) Adduct by High-Performance Liquid Chromatography (HPLC):** The DA-RV adduct was purified using a C18 column in an Agilent Technologies 1260 Infinity II LC System (Santa Clara, CA, USA). Solvent A was water with 0.1% trifluoroacetic acid (TFA), and solvent B was acetonitrile (0.1% TFA). The full gradient is provided in the supporting information (Figure S6). Samples were filtered through a syringe-driven 0.22 um PVDF filter before injection. UV-Vis absorbance was monitored at three wavelengths: 286 nm, 304 nm, and 425 nm. The 425 nm wavelength corresponded to the dopamine-resveratrol adduct. A peak appeared in the 425 nm channel 22.7 min into the gradient, corresponding to 36.8% Solvent B. The product was collected starting at 22 min elution time until the peak had fully diminished. The collected fluid appeared as a bright yellow-green solution.

**Characterization of DA-RV Adduct:** UV-Vis absorbance spectra of the dopamine-resveratrol adduct were obtained using a UV2600 spectrophotometer (Shimadzu Scientific Instruments, Kyoto, Japan). High-resolution mass spectrometry analysis was performed with electrospray ionization mass spectrometry (ESI-MS) on a Thermo LTQ-FT instrument at the QB3 core facility (UC Berkeley). Additional absorbance ($\lambda_{abs}$ = 310–600 nm) and fluorescence emission scans ($\lambda_{ex}$ = 390 nm, $\lambda_{em}$ = 415–750 nm) were collected on a Tecan Infinite M200 plate reader at 0.02 mg/mL adduct in various solvents (see supporting information). Fourier transform infrared (FTIR) spectra were collected on a Bruker Vertex

80 FTIR spectrometer equipped with an attenuated total reflectance accessory with a diamond window (LBNL Catalysis Facility, UC Berkeley). $^{1}$-, $^{13}$C-NMR, and $^{1}$H spectra were collected on a Bruker 900 MHz instrument equipped with a cryoprobe at the Central California 900 MHz NMR facility at UC Berkeley. $^{1}$H NMR (900 MHz, DMSO-$d_6$) δ 10.86 (s, 1H), 9.81 (s, 1H), 9.41 (bs, 2H), 7.85 (bs, 1H), 7.53 (d, $J$ = 8.6 Hz, 2H), 7.21 (d, $J$ = 16.1 Hz, 1H), 7.18 (d, $J$ = 16.0 Hz, 1H), 6.82 (d, $J$ = 8.5 Hz, 2H), 6.80 (d, $J$ = 1.9 Hz, 1H), 6.38 (d, $J$ = 2.0 Hz, 1H), 6.36 (s, 1H), 3.28 (app dd, $J$ = 14.0, $J$ = 5.6 Hz, 1H), 3.12 (app td, $J$ = 13.7, $J$ = 4.2 Hz, 1H), 2.70 (d, $J$ = 12.0 Hz, 1H), 2.61 (dd, $J$ = 11.9, 2.3 Hz, 1H), 2.16 (app td, $J$ = 13.4, 5.7 Hz, 1H), 1.82 (app d, $J$ = 13.2 Hz, 1H). $^{13}$C NMR (226 MHz, DMSO-$d_6$) δ 188.61, 166.09, 165.20, 164.14, 158.37, 139.91, 134.07, 128.89, 127.20, 120.09, 115.74, 113.48, 110.29, 107.66, 96.66, 86.79, 82.77, 43.48, 36.44, 29.13. Graphical spectra are presented in supporting information.

### 2.4. Nanoparticle Characterization

**Spectroscopic Characterization:** UV-Vis absorbance spectra were obtained using a UV2600 spectrophotometer (Shimadzu Scientific Instruments, Kyoto, Japan). To calculate extinction coefficients, a UV-Vis absorbance plate reader (Infinite M200 Pro, Tecan Trading AG, Switzerland) was used to facilitate high-throughput analysis. For extinction coefficient quantification, PDA and RV@PDA were diluted to concentrations of 1, 2, 5, 10, 20, and 50 μg/mL. The UV-Vis absorbances of these solutions were then measured in triplicate and averaged. The curve of absorbance vs. concentration was then fit to a linear relation according to Beer's law ($A = \varepsilon bc$) at $\lambda_{abs}$ = 400 nm, 500 nm, 600 nm, 700 nm, 800 nm, 900 nm, and 977 nm, where A is the absorbance of the sample, c is the concentration in μg/mL, b is the path length in cm, and ε is the extinction coefficient in $cm^{-1} * (\mu g/mL)^{-1}$. All linear fits with $r^2 \geq 0.94$ were obtained except for RV@PDA grown in 1:1 RV:DA solution at $\lambda_{abs}$ = 800 nm ($r^2$ = 0.89), 900 nm ($r^2$ = 0.88), and 977 nm ($r^2$ = 0.83).

**Dynamic Light Scattering and Zeta Potential Analysis:** Dynamic light scattering (DLS) and zeta potential analysis of PDA and RV@PDA nanostructures was conducted using a Malvern Zetasizer Nano ZS instrument (Malvern, Worcestershire, UK). The hydrodynamic diameter ($D_h$) of each batch of NPs or NCs was taken as the z-average particle diameter obtained from cumulants analysis by the Malvern Zetasizer software. During zeta potential measurement, pH was controlled with 10 mM citrate buffer (pH 2.5 – 6.5), 10 mM HEPES buffer (pH 7.0 – 7.5), or 10 mM bicine buffer (pH 8.0 – 9.0). Zeta potential was calculated by the Malvern Zetasizer software utilizing the method detailed by Wiersma et al. using the Smoluchowski approximation ($f_1(\varkappa a) = 1.5$).[51]

**Electron Microscopy Imaging:** Conventional transmission electron microscopy (TEM) imaging was performed on an FEI Tecnai 12 TEM (Hillsboro, OR, USA). Samples were prepared by dropping 5 μL of PDA or RV@PDA suspension onto a carbon film-coated 400 mesh copper TEM grid (Electron Microscopy Sciences, Hatfield, PA, USA) and rinsing with UP water. Scanning electron microscopy (SEM) images were obtained using an FEI Quanta 3D FEG SEM (Hillsboro, OR, USA). SEM samples were sputter coated with 20 nm of gold to prevent charging. The images were taken at a beam voltage of 10 kV and current of 0.33

nA. Freeze fracturing of SEM samples was performed by freezing drop-casted NPs in liquid nitrogen before striking them with a hammer.

**X-ray Photoelectron Spectroscopy (XPS):** XPS samples were prepared as we have previously described.[24] Substrates were cleaned by serial sonication in ultrapure water, acetone, and isopropanol for 10 min each followed by plasma cleaning at 60 W for 10 min (Harrick Plasma Cleaner, Ithaca, NY, USA). Then, 20-50 $\mu$L droplets of concentrated PDA or RV@PDA suspensions (~ 0.25-1 mg/mL) were placed onto clean gold-coated silicon substrates and dried overnight. Substrates were dried completely under high vacuum prior to analysis in a PHI 5600 spectrometer (PerkinElmer) equipped with an Al monochromated 2 mm filament and a built-in charge neutralizer. The X-ray source operated at 350 W, 14.8 V, and 40° take-off angle. The atomic concentrations (atom %) of nitrogen, oxygen, and carbon of drop-casted nanomaterial was determined relative to total nitrogen, oxygen, and carbon content by performing survey scans between 0 and 1100 eV electron binding energies. Charge correction was performed setting the C1s peak at 285.0 eV. Data analysis was conducted using MultiPak software version 9.6.015 (Physical Electronics, Chanhassen, MN, USA) and OriginPro 2017 software (Student version, OriginLab, Northampton, MA, USA).

**DPPH Free Radical Scavenging Assay:** To measure antioxidant activity of the PDA and RV@PDA, a DPPH assay was adapted from the literature for use on a UV-Vis absorbance plate reader (Synergy H1, BioTek, Winooski, VT, USA).[52] Briefly, between 0 and 50 μg/mL of antioxidant (PDA, RV@PDA, RV, DA, or ascorbic acid) were mixed with 100 μM DPPH in ethanol. Trace water was present in wells containing DA to improve solubility (<10 vol %). The scavenging of DPPH was observed by monitoring absorbance of the DPPH radical at $\lambda_{abs}$ = 517 nm from 5 min – 60 min. In order to control for the background absorbance of each antioxidant, the absorbances of each well containing DPPH and antioxidant were subtracted by the absorbances of wells containing the antioxidant dissolved in ethanol without DPPH. As the initial free radical of DPPH was converted to DPPH-H, the absorbance at 517 nm decreased. Fraction of DPPH remaining was calculated using absorbance at 517 nm at a given time and the initial absorbance at 517 nm. Measurements were performed in triplicate.

### 2.5. Statistical Analysis

Statistical analysis was performed in Minitab 17 (Minitab Inc., State College, PA, USA) by conducting ANOVA followed by post-hoc Tukey tests. All error bars represent standard deviations (SD) of at least three samples unless otherwise noted.

## 3. Results and Discussion

### 3.1. Preparation of PDA and RV@PDA

To prepare RV@PDA, an ethanolic RV solution (12.5 mg/mL) was first added into a 5:1 water:ethanol mixture (Figure 1). Immediately after mixing, light scattering (derived count rate = 247 kcps by DLS) indicated that either emulsion or nanoprecipitate formation occurred, possibly driven by the poor water solubility of RV (0.03 mg/mL).[53] The addition of dopamine·HCl (DA) to this mixture accompanied by neutralization of the solution pH to

8.5 resulted in a darkening of the color of the solution, qualitatively indicating the formation of PDA. To prepare the RV-free PDA control, the first step of RV addition into growth solution was omitted.

The effects of solvent composition and particle growth time on hydrodynamic diameter ($D_h$) were evaluated by *in situ* DLS analysis of solutions containing 0.125 mg/mL RV and 0.25 mg/mL DA. Over approximately the first six hours of particle growth, it was not possible to measure $D_h$ by DLS due to significant polydispersity. Between 7 h and 24 h of growth, it was observed that $D_h$ of RV@PDA increased for solvent compositions of 3:1 – 12:1 water:ethanol (Figure S1). The final diameters ranged from 109 nm to 222 nm after 24 h and were lower at higher water:ethanol ratios (Figure S1). The 5:1 water:ethanol solvent composition and 24 h growth time was utilized for subsequent experiments.

The optical density of the final solutions inversely correlated with the RV:DA mass ratio, with solutions containing DA alone darkest and solutions containing RV alone lightest (Figure 2a). No darkening occurred in RV solutions with or without DA when the pH of the solution was not adjusted to pH 8.5, indicating that basic conditions were required in order to form nanoparticles (Figure S2). The overall mass of PDA and RV@PDA isolated from the growth solutions decreased as RV:DA mass ratio increased, suggesting that RV interferes with PDA growth in some manner. This result is consistent with the partial consumption of RV and DA to form soluble fluorescent byproduct (see section 3.2).

Nanoparticles prepared from pure DA exhibited a PDA-like broadband UV-Vis absorbance that monotonically decayed with increasing wavelengths (Figures 2b, S3, S4), consistent with what has been reported previously for PDA.[23-24, 26] On the other hand, the UV-Vis absorbance spectra of purified RV@PDA prepared from solutions containing DA and RV had an absorbance peak at $\lambda_{abs}$ = 305 nm superimposed on the PDA-like broadband absorbance spectra (Figure 2b). This distinctive absorbance peak at 305 nm is consistent with that of RV, suggesting that RV is incorporated into RV@PDA product. The extinction coefficients of the PDA and RV@PDA nanoparticles decreased as more RV was added into the growth solutions, showing that RV@PDA are less intensely absorbing than pure PDA (Figure S4, Table S1). This result suggests that RV incorporation into RV@PDA may disrupt the highly conjugated, optically absorbent PDA structure. No broadband absorbance occurred in solutions that did not contain DA or pH 8.5 buffer (Figure S2).

Zeta potential measurements on pure PDA and RV@PDA nanoparticles grown at 0.5:1 RV:DA were measured at a range of pH values from 2.5 to 9.5 (Figure 3a). The pH-dependence of zeta potential matches closely with published results on PDA, with the isoelectric point of both PDA and RV@PDA lying between pH 4.0 and pH 4.5.[24] This result suggests that the surface charge of the nanoparticles is governed primarily by PDA.

As expected for PDA and RV@PDA, XPS scans of drop-cast PDA and RV@PDA nanoparticles all have peaks corresponding to O 1s at ~533 eV, C 1s at ~285 eV, and N 1s at ~400 eV (Figure 3b). Atomic ratio analysis from high resolution O 1s, C 1s, and N 1s scans (Figure 3c-d, Figure S5) reveal trends in C and N at% consistent with incorporation of RV into the PV@PDA nanoparticles. The lack of significant differences between the C and N

composition of RV@PDA prepared at 0.5:1 RV:DA and 1:1 RV:DA may indicate that the RV content of RV@PDA nanomaterials has a saturation limit, beyond which additional RV incorporation does not occur. Deconvoluted high resolution XPS scans of the C 1s and O 1s peaks of PDA and RV@PDA prepared at 0.5:1 and 1:1 RV:DA provide further support for RV incorporation (Figure S5).

### 3.2. DA-RV Adduct Formation

We noted earlier that growth solutions of RV@PDA became a distinctive yellow-green color over the course of 24 h, which was not observed in reaction solutions containing only DA or only RV at pH 8.5 (Figure 2a). The supernatants recovered from RV@PDA growth solutions following centrifugation had a UV-Vis absorbance peak at $\lambda_{abs}$ = 420 nm in addition to the absorbance peak at $\lambda_{abs}$ = 309 nm associated with RV (Figure 4d, S3b). We hypothesized that this peak represented an azamonardine-type chromophore formed by the reaction of DA and RV (Figure 4a). Semi-preparative reverse phase HPLC of both 0.5:1 and 1:1 RV:DA grown solution supernatants revealed a single major peak with strong absorbance at 425 nm (Figure S6). The pure product, isolated as a bright yellow trifluoroacetate salt, demonstrated two distinct UV-Vis absorbance peaks, at $\lambda_{abs}$ = 309 nm and $\lambda_{abs}$ = 398 nm (Figure S7), and solutions in DMSO were fluorescent under UV excitation (Figures S8-S10). Analysis by high resolution electrospray ionization mass spectrometry (ESI-MS) in positive and negative ion modes revealed peaks at 378.1336 m/z and 376.1184 m/z, respectively, corresponding to a parent molecular formula $C_{22}H_{19}NO_5$ (Figure 4b). These results are consistent with a 1:1 adduct between dopamine and resveratrol with a degree of unsaturation of 14.

Further analyses of the adduct by $^{1}H$- and $^{13}C$-NMR spectrometry, as well as $^{1}H$-$^{13}C$ HSQC and HMBC experiments, and infrared spectrometry support the formation of an azamonardine moiety with the proposed structure shown in Figure 4a (Figures S11-S15). This structure is analogous to the previously described monardine and azamonardine fluorophores formed between resorcinol and either 3,4-dihydroxyphenethyl alcohol or dopamine, respectively, under mildly basic conditions (pH >8) in the presence of dissolved oxygen at room temperature.[54-55] These conditions are similar to the nanomaterial growth conditions used in our work.

The UV-Vis absorbance peak shift of the DA-RV adduct is consistent with the findings of Acuña et al., who observed that azamonardine has an absorbance maximum at $\lambda_{abs}$ = 389 nm at pH 6 and $\lambda_{abs}$ = 419 nm at pH 9.[55] These peaks are close to the higher wavelength absorbance maxima of the DA-RV adduct peaks at $\lambda_{abs}$ = 398 nm following purification via HPLC under acidic conditions and $\lambda_{abs}$ = 425 nm in the pH 8.5 supernatant of the nanomaterial synthesis. The presence of a second strong absorbance peak in the DA-RV molecule at 309 nm suggests that the 4-hydroxystyryl fragment of the DA-RV adduct is not fully conjugated with the azamonardine moiety, and is likely out of the plane of the conjugated system derived from dopamine and the resorcinol fragment of RV. Furthermore, the DA-RV adduct fluorescence emission intensity is pH dependent, with a maximum emission intensity at 495 nm observed at pH 8.5 ($\lambda_{ex}$ = 390 nm) among the buffer pH values examined (Figure 4c). This behavior is consistent with the pH-dependent absorbance and

fluorescence properties of azamonardine fluorophores that have been previously reported by both Acuna and Zhang.[54-55]

The azamonardine scaffold presumably forms first by trapping of the highly reactive dopamine quinone by resveratrol (Figure S16). At low concentrations of reactants, this substitution occurs quickly enough that it competes with formation of aminochrome and dihydroxyindole from dopamine[55], essential intermediates for PDA generation, potentially explaining the reduced yield of RV@PDA relative to PDA. Following electrophilic substitution of resveratrol and additional oxidation of the DA fragment, cyclization by Michael addition of a pendant phenol of the RV fragment onto the DA carbon bearing the aminoethyl moiety can occur. Subsequent tautomerization enables nucleophilic addition by the pendant amine to the proximal ketone, forming the hemiaminal characteristic of the azamonardine fluorophores (Figure S16).

### 3.3. Morphology of RV@PDA Nanostructures

The RV@PDA morphologies were evaluated by TEM and SEM. PDA nanoparticles formed in the absence of RV were found to be predominantly solid and spherical. In contrast, increasing the RV:DA ratio in the growth solution from 0:1 to 0.5:1 RV:DA resulted in increased nanocapsule formation as indicated by TEM (Figure 5a-c). At 0.5:1 RV:DA, the product was predominantly NCs. As the RV:DA ratio was further increased to 1:1, the NCs have thinner shells and more irregular appearances. Some NCs appear to deform during synthesis or in the high vacuum environment of the EM (Figure 5d). At 2:1 RV:DA, low electron-contrast nanoparticles were observed by TEM (data not shown), which may indicate the presence of resveratrol aggregates rather than electron-dense polydopamine.

SEM images show that the outer surfaces of the PDA and RV@PDA nanostructures are smooth and spherical (0:1 and 0.5:1 RV:DA, Figure 6a,b). SEM micrographs of freeze-fractured RV@PDA (0.5:1 RV:DA) reveal that the inner core is hollow, consistent with a nanocapsule morphology (Figure 6c). It is possible that this morphology reflects the initial formation of RV nanoparticles due to low solubility in the growth medium, followed subsequently by deposition of a dense PDA shell.

### 3.4. RV@PDA Nanocapsule Diameter and Shell Thickness Control by DA Concentration

The diameter and shell thickness of the RV@PDA particles were tunable through DA concentration. At a constant 0.25 mg/mL RV concentration in the growth solution, TEM analysis of particles revealed a general trend toward greater overall diameter and shell thickness with increasing DA concentration ≥ 0.25 mg/mL (Figure 7). Particle diameter increased with DA concentration, with $D_h$ = 221.6 ± 40.4 nm for 0.25 mg/mL DA (1:1 RV:DA), 319.7 ± 16.6 nm for 0.50 mg/mL DA (0.5:1 RV:DA), and 471.6 ± 26.3 nm for 1.00 mg/mL DA (0.25:1 RV:DA). The shell thickness of NCs increased from ~10 nm at 0.25 mg/mL DA (1:1 RV:DA) to ~100 nm at 1.00 mg/mL DA (0.25:1 RV:DA). These results indicate that the predominant effect of additional DA in solution is to increase PDA shell thickness.

### 3.5. Antioxidant Activity of RV@PDA NCs

Using a DPPH assay, the antioxidant activities of both PDA NPs and RV@PDA NCs were evaluated by monitoring the reduction of DPPH radicals (Figure 8). PDA NPs were prepared in 0.25 mg/mL DA solution, and RV@PDA NCs were prepared in 0.125 mg/mL RV, 0.25 mg/mL DA solution (0.5:1 RV:DA). Free RV, DA, and ascorbic acid were used as controls. The antioxidant performance of RV@PDA NCs was better than both DA and RV alone at 5 min over the 5—50 μg/mL concentration regime (Figure 8a). At 60 min, the antioxidant activity of RV@PDA NCs was comparable to that of DA and remained greater than that of RV (Figure 8b). Furthermore, the antioxidant activity of RV@PDA NCs is not significantly different from that of ascorbic acid at concentrations of ≥ 20 μg/mL at 60 min.

## 4. Conclusions

In this work, we have demonstrated a novel technique to synthesize PDA nanocapsules (NCs) without the use of nanoparticle templates. In this approach, the presence of the hydrophobic stilbene resveratrol (RV) during auto-oxidative formation of PDA induces nanocapsule formation and incorporation of RV in the NCs, as confirmed by UV-Vis spectroscopy and XPS. The surfaces of RV@PDA NCs have zeta potentials similar to PDA NPs, indicating that the surface ionization is governed predominantly by PDA. Although more studies of the formation mechanism are needed, our data suggest that NC formation is triggered by nanoscale aggregation of RV followed by stabilization with and overgrowth of PDA. Additionally, a fluorescent azamonardine adduct is formed between RV and DA during NP synthesis. The morphology, shell thickness and diameters of RV@PDA NCs was dependent on the RV:DA mass ratio in growth solution, and the RV@PDA NCs have excellent antioxidant activity. The convenient approach to nanocapsule synthesis detailed in this work may prove useful in the encapsulation of other hydrophobic cargo, such as other bioactive phenols and chemotherapeutic drugs. Furthermore, the demonstrated chemical versatility of the resulting PDA shell can be exploited for convenient post-functionalization with biomolecules, enabling applications such as targeted drug delivery or imaging.

## Supplementary Material

Refer to Web version on PubMed Central for supplementary material.

## Acknowledgements

This work was supported by NIH grant R37 DE014193. D.R.A. acknowledges support from NIH grants T32GM008152 and T32GM008449. A.B.K. acknowledges support from the National Science Foundation Graduate Research Fellowship Program under grant DGE 1752814. This work used the Electron Microscopy Lab at UC Berkeley. We thank Prof. Haeshin Lee for insightful discussion. We thank Jeffrey G. Pelton at the Central California 900 MHz NMR Facility at UC Berkeley for assistance with NMR experiments. Funds for the 900 MHz NMR spectrometer were provided by the NIH through grant GM68933.

## References

1. Lee H; Dellatore SM; Miller WM; Messersmith PB, Mussel-inspired surface chemistry for multifunctional coatings. Science 2007, 318 (5849), 426–430. [PubMed: 17947576]

2. Liu MY; Zeng GJ; Wang K; Wan Q; Tao L; Zhang XY; Wei Y, Recent developments in polydopamine: an emerging soft matter for surface modification and biomedical applications. Nanoscale 2016, 8 (38), 16819–16840. [PubMed: 27704068]
3. Liu Y; Ai K; Lu L, Polydopamine and Its Derivative Materials: Synthesis and Promising Applications in Energy, Environmental, and Biomedical Fields. Chem. Rev 2014, 114 (9), 5057–5115. [PubMed: 24517847]
4. Ryu JH; Messersmith PB; Lee H, Polydopamine Surface Chemistry: A Decade of Discovery. ACS Applied Materials & Interfaces 2018, 10 (9), 7523–7540. [PubMed: 29465221]
5. Chen C-T; Martin-Martinez FJ; Jung GS; Buehler MJ, Polydopamine and eumelanin molecular structures investigated with ab initio calculations. Chemical Science 2017.
6. Hong S; Na YS; Choi S; Song IT; Kim WY; Lee H, Non-Covalent Self-Assembly and Covalent Polymerization Co-Contribute to Polydopamine Formation. Adv Funct Mater 2012, 22 (22), 4711–4717.
7. Liebscher J; Mrówczyński R; Scheidt HA; Filip C; Hădade ND; Turcu R; Bende A; Beck S, Structure of Polydopamine: A Never-Ending Story? Langmuir 2013, 29 (33), 10539–10548. [PubMed: 23875692]
8. Dreyer DR; Miller DJ; Freeman BD; Paul DR; Bielawski CW, Elucidating the Structure of Poly(dopamine). Langmuir 2012, 28 (15), 6428–6435. [PubMed: 22475082]
9. Della Vecchia NF; Avolio R; Alfè M; Errico ME; Napolitano A; d'Ischia M, Building-Block Diversity in Polydopamine Underpins a Multifunctional Eumelanin-Type Platform Tunable Through a Quinone Control Point. Adv. Funct. Mater 2013, 23 (10), 1331–1340.
10. Lynge ME; van der Westen R; Postma A; Stadler B, Polydopamine-a nature-inspired polymer coating for biomedical science. Nanoscale 2011, 3 (12), 4916–4928. [PubMed: 22024699]
11. Lee H; Rho J; Messersmith PB, Facile Conjugation of Biomolecules onto Surfaces via Mussel Adhesive Protein Inspired Coatings. Advanced Materials 2009, 21 (4), 431–434. [PubMed: 19802352]
12. Black KCL; Yi J; Rivera JG; Zelasko-Leon DC; Messersmith PB, Polydopamine-enabled surface functionalization of gold nanorods for cancer cell-targeted imaging and photothermal therapy. Nanomedicine 2013, 8 (1), 17–28. [PubMed: 22891865]
13. Zelasko-Leon DC; Fuentes CM; Messersmith PB, MUC1-Targeted Cancer Cell Photothermal Ablation Using Bioinspired Gold Nanorods. PLoS One 2015, 10 (7), 20.
14. Wang S; Zhao X; Wang S; Qian J; He S, Biologically Inspired Polydopamine Capped Gold Nanorods for Drug Delivery and Light-Mediated Cancer Therapy. ACS Applied Materials & Interfaces 2016, 8 (37), 24368–24384. [PubMed: 27564325]
15. Zhou JJ; Xiong QR; Ma JL; Ren JH; Messersmith PB; Chen P; Duan HW, Polydopamine-Enabled Approach toward Tailored Plasmonic Nanogapped Nanoparticles: From Nanogap Engineering to Multifunctionality. ACS Nano 2016, 10 (12), 11066–11075. [PubMed: 28024348]
16. Choi CKK; Li J; Wei K; Xu YJ; Ho LWC; Zhu M; To KKW; Choi CHJ; Bian L, A Gold@Polydopamine Core–Shell Nanoprobe for Long-Term Intracellular Detection of MicroRNAs in Differentiating Stem Cells. Journal of the American Chemical Society 2015, 137 (23), 7337–7346. [PubMed: 25996312]
17. Liao N; Wu M; Pan F; Lin J; Li Z; Zhang D; Wang Y; Zheng Y; Peng J; Liu X; Liu J, Poly (dopamine) coated superparamagnetic iron oxide nanocluster for noninvasive labeling, tracking, and targeted delivery of adipose tissue-derived stem cells. Scientific Reports 2016, 6, 18746. [PubMed: 26728448]
18. Wei Y; Gao L; Wang L; Shi L; Wei E; Zhou B; Zhou L; Ge B, Polydopamine and peptide decorated doxorubicin-loaded mesoporous silica nanoparticles as a targeted drug delivery system for bladder cancer therapy. Drug Delivery 2017, 24 (1), 681–691. [PubMed: 28414557]
19. Zhao H; Chao Y; Liu J; Huang J; Pan J; Guo W; Wu J; Sheng M; Yang K; Wang J; Liu Z, Polydopamine Coated Single-Walled Carbon Nanotubes as a Versatile Platform with Radionuclide Labeling for Multimodal Tumor Imaging and Therapy. Theranostics 2016, 6 (11), 1833–43. [PubMed: 27570554]
20. Fei B; Qian B; Yang Z; Wang R; Liu WC; Mak CL; Xin JH, Coating carbon nanotubes by spontaneous oxidative polymerization of dopamine. Carbon 2008, 46 (13), 1795–1797.

21. Park J; Brust TF; Lee HJ; Lee SC; Watts VJ; Yeo Y, Polydopamine-Based Simple and Versatile Surface Modification of Polymeric Nano Drug Carriers. ACS Nano 2014, 8 (4), 3347–3356. [PubMed: 24628245]
22. Sunoqrot S; Hasan L; Alsadi A; Hamed R; Tarawneh O, Interactions of mussel-inspired polymeric nanoparticles with gastric mucin: Implications for gastro-retentive drug delivery. Colloids and surfaces. B, Biointerfaces 2017, 156, 1–8. [PubMed: 28499200]
23. Ju K-Y; Lee Y; Lee S; Park SB; Lee J-K, Bioinspired Polymerization of Dopamine to Generate Melanin-Like Nanoparticles Having an Excellent Free-Radical-Scavenging Property. Biomacromolecules 2011, 12 (3), 625–632. [PubMed: 21319809]
24. Amin D; Sugnaux C; Lau K; Messersmith P, Size Control and Fluorescence Labeling of Polydopamine Melanin-Mimetic Nanoparticles for Intracellular Imaging. Biomimetics 2017, 2 (3), 17. [PubMed: 29360110]
25. Yan J; Yang L; Lin M-F; Ma J; Lu X; Lee PS, Polydopamine Spheres as Active Templates for Convenient Synthesis of Various Nanostructures. Small 2013, 9 (4), 596–603. [PubMed: 23117928]
26. Liu Y; Ai K; Liu J; Deng M; He Y; Lu L, Dopamine-Melanin Colloidal Nanospheres: An Efficient Near-Infrared Photothermal Therapeutic Agent for In Vivo Cancer Therapy. Advanced Materials 2013, 25 (9), 1353–1359. [PubMed: 23280690]
27. Dong Z; Gong H; Gao M; Zhu W; Sun X; Feng L; Fu T; Li Y; Liu Z, Polydopamine Nanoparticles as a Versatile Molecular Loading Platform to Enable Imaging-guided Cancer Combination Therapy. Theranostics 2016, 6 (7), 1031–42. [PubMed: 27217836]
28. Li WQ; Wang Z; Hao S; He H; Wan Y; Zhu C; Sun LP; Cheng G; Zheng SY, Mitochondria-Targeting Polydopamine Nanoparticles To Deliver Doxorubicin for Overcoming Drug Resistance. ACS Applied Materials & Interfaces 2017, 9 (20), 16793–16802. [PubMed: 28481505]
29. Huang Y; Li Y; Hu Z; Yue X; Proetto MT; Jones Y; Gianneschi NC, Mimicking Melanosomes: Polydopamine Nanoparticles as Artificial Microparasols. ACS Central Science 2017, 3 (6), 564–569. [PubMed: 28691067]
30. Rosler A; Vandermeulen GWM; Klok HA, Advanced drug delivery devices via self-assembly of amphiphilic block copolymers. Advanced Drug Delivery Reviews 2012, 64, 270–279.
31. Mahapatro A; Singh DK, Biodegradable nanoparticles are excellent vehicle for site directed in-vivo delivery of drugs and vaccines. Journal of Nanobiotechnology 2011, 9, 11. [PubMed: 21443799]
32. Miladi K; Sfar S; Fessi H; Elaissari A, Nanoprecipitation Process: From Particle Preparation to In Vivo Applications In Polymer Nanoparticles for Nanomedicines: A Guide for their Design, Preparation and Development, Vauthier C; Ponchel G, Eds. Springer International Publishing: Cham, 2016; pp 17–53.
33. Yow HN; Routh AF, Formation of liquid core-polymer shell microcapsules. Soft Matter 2006, 2 (11), 940–949.
34. Anton N; Benoit JP; Saulnier P, Design and production of nanoparticles formulated from nano-emulsion templates - A review. J. Control. Release 2008, 128 (3), 185–199. [PubMed: 18374443]
35. Karim R; Palazzo C; Evrard B; Piel G, Nanocarriers for the treatment of glioblastoma multiforme: Current state-of-the-art. J. Control. Release 2016, 227, 23–37. [PubMed: 26892752]
36. Yang X-C; Samanta B; Agasti SS; Jeong Y; Zhu Z-J; Rana S; Miranda OR; Rotello VM, Drug Delivery Using Nanoparticle-Stabilized Nanocapsules. Angewandte Chemie International Edition 2011, 50 (2), 477–481. [PubMed: 21154794]
37. Tang R; Kim CS; Solfiell DJ; Rana S; Mout R; Velázquez-Delgado EM; Chompoosor A; Jeong Y; Yan B; Zhu Z-J; Kim C; Hardy JA; Rotello VM, Direct Delivery of Functional Proteins and Enzymes to the Cytosol Using Nanoparticle-Stabilized Nanocapsules. ACS Nano 2013, 7 (8), 6667–6673. [PubMed: 23815280]
38. Postma A; Yan Y; Wang Y; Zelikin AN; Tjipto E; Caruso F, Self-Polymerization of Dopamine as a Versatile and Robust Technique to Prepare Polymer Capsules. Chemistry of Materials 2009, 21 (14), 3042–3044.
39. Liu Q; Yu B; Ye W; Zhou F, Highly selective uptake and release of charged molecules by pH-responsive polydopamine microcapsules. Macromol Biosci 2011, 11 (9), 1227–34. [PubMed: 21721126]

40. Cui J; Yan Y; Such GK; Liang K; Ochs CJ; Postma A; Caruso F, Immobilization and Intracellular Delivery of an Anticancer Drug Using Mussel-Inspired Polydopamine Capsules. Biomacromolecules 2012, 13 (8), 2225–2228. [PubMed: 22792863]
41. Chen X; Yan Y; Müllner M; van Koeverden MP; Noi KF; Zhu W; Caruso F, Engineering Fluorescent Poly(dopamine) Capsules. Langmuir 2014, 30 (10), 2921–2925. [PubMed: 24597595]
42. Ni Y-Z; Jiang W-F; Tong G-S; Chen J-X; Wang J; Li H-M; Yu C-Y; Huang X.-h.; Zhou Y-F, Preparation of polydopamine nanocapsules in a miscible tetrahydrofuran-buffer mixture. Organic & Biomolecular Chemistry 2015, 13 (3), 686–690. [PubMed: 25424983]
43. Han P; Jiang Z; Wang X; Wang X; Zhang S; Shi J; Wu H, Facile preparation of porous magnetic polydopamine microspheres through an inverse replication strategy for efficient enzyme immobilization. Journal of Materials Chemistry B 2015, 3 (36), 7194–7202.
44. Shi J; Yang C; Zhang S; Wang X; Jiang Z; Zhang W; Song X; Ai Q; Tian C, Polydopamine Microcapsules with Different Wall Structures Prepared by a Template-Mediated Method for Enzyme Immobilization. Acs Applied Materials & Interfaces 2013, 5 (20), 9991–9997. [PubMed: 24059356]
45. Shi J; Zhang W; Zhang S; Wang X; Jiang Z, Synthesis of organic-inorganic hybrid microcapsules through in situ generation of an inorganic layer on an adhesive layer with mineralization-inducing capability. Journal of Materials Chemistry B 2015, 3 (3), 465–474.
46. Cui JW; Wang YJ; Postma A; Hao JC; Hosta-Rigau L; Caruso F, Monodisperse Polymer Capsules: Tailoring Size, Shell Thickness, and Hydrophobic Cargo Loading via Emulsion Templating. Adv. Funct. Mater 2010, 20 (10), 1625–1631.
47. Xu H; Liu X; Wang D, Interfacial Basicity-Guided Formation of Polydopamine Hollow Capsules in Pristine O/W Emulsions – Toward Understanding of Emulsion Template Roles. Chemistry of Materials 2011, 23 (23), 5105–5110.
48. Jang M; Cai L; Udeani GO; Slowing KV; Thomas CF; Beecher CWW; Fong HHS; Farnsworth NR; Kinghorn AD; Mehta RG; Moon RC; Pezzuto JM, Cancer Chemopreventive Activity of Resveratrol, a Natural Product Derived from Grapes. Science 1997, 275 (5297), 218–220. [PubMed: 8985016]
49. Mohar DS; Malik S, The Sirtuin System: The Holy Grail of Resveratrol? Journal of Clinical & Experimental Cardiology 2012, 3 (11), 216. [PubMed: 23560248]
50. Baur JA; Pearson KJ; Price NL; Jamieson HA; Lerin C; Kalra A; Prabhu VV; Allard JS; Lopez-Lluch G; Lewis K; Pistell PJ; Poosala S; Becker KG; Boss O; Gwinn D; Wang M; Ramaswamy S; Fishbein KW; Spencer RG; Lakatta EG; Le Couteur D; Shaw RJ; Navas P; Puigserver P; Ingram DK; de Cabo R; Sinclair DA, Resveratrol improves health and survival of mice on a high-calorie diet. Nature 2006, 444 (7117), 337–342. [PubMed: 17086191]
51. Wiersema PH; Loeb AL; Overbeek JTG, Calculation of the electrophoretic mobility of a spherical colloid particle. Journal of Colloid and Interface Science 1966, 22 (1), 78–99.
52. Brand-Williams W; Cuvelier ME; Berset C, Use of a Free-Radical Method to Evaluate Antioxidant Activity. Food Science and Technology-Lebensmittel-Wissenschaft & Technologie 1995, 28 (1), 25–30.
53. Amri A; Chaumeil JC; Sfar S; Charrueau C, Administration of resveratrol: What formulation solutions to bioavailability limitations? J. Control. Release 2012, 158 (2), 182–193. [PubMed: 21978644]
54. Zhang X; Zhu Y; Li X; Guo X; Zhang B; Jia X; Dai B, A simple, fast and low-cost turn-on fluorescence method for dopamine detection using in situ reaction. Analytica chimica acta 2016, 944 (Supplement C), 51–56. [PubMed: 27776639]
55. Acuna AU; Alvarez-Perez M; Liras M; Coto PB; Amat-Guerri F, Synthesis and photophysics of novel biocompatible fluorescent oxocines and azocines in aqueous solution. Physical Chemistry Chemical Physics 2013, 15 (39), 16704–16712. [PubMed: 23986088]

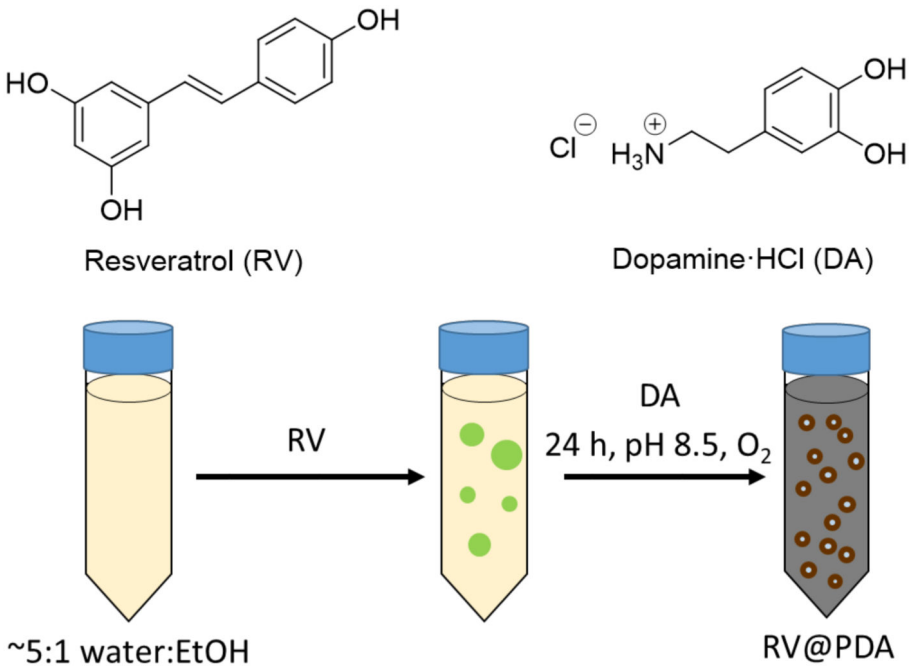


**Figure 1:**
Chemical structures of DA and RV, and experimental method for RV@PDA preparation. PDA was prepared by omitting the addition of RV into growth solution.

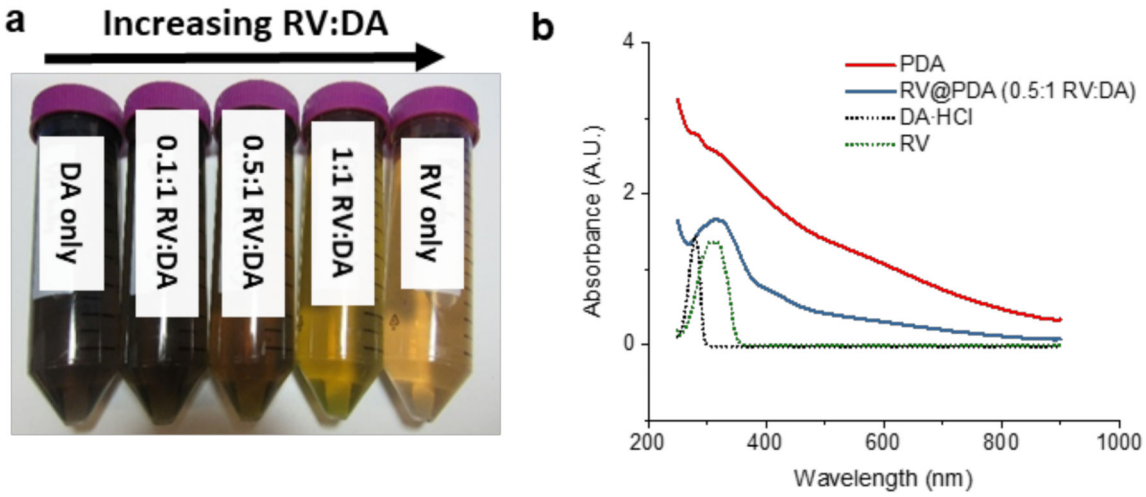


**Figure 2:**

Optical characterization of PDA and RV@PDA. (**a**) Appearance of growth solutions containing 0.25 mg/mL DA containing 0.1:1, 0.5:1, and 1:1 RV:DA versus 0.25 mg/mL DA and 0.25 mg/mL RV after 24 h. (**b**) UV-Vis absorbance spectra of pure PDA and RV@PDA. Spectra of DA and RV only are also shown for comparison.

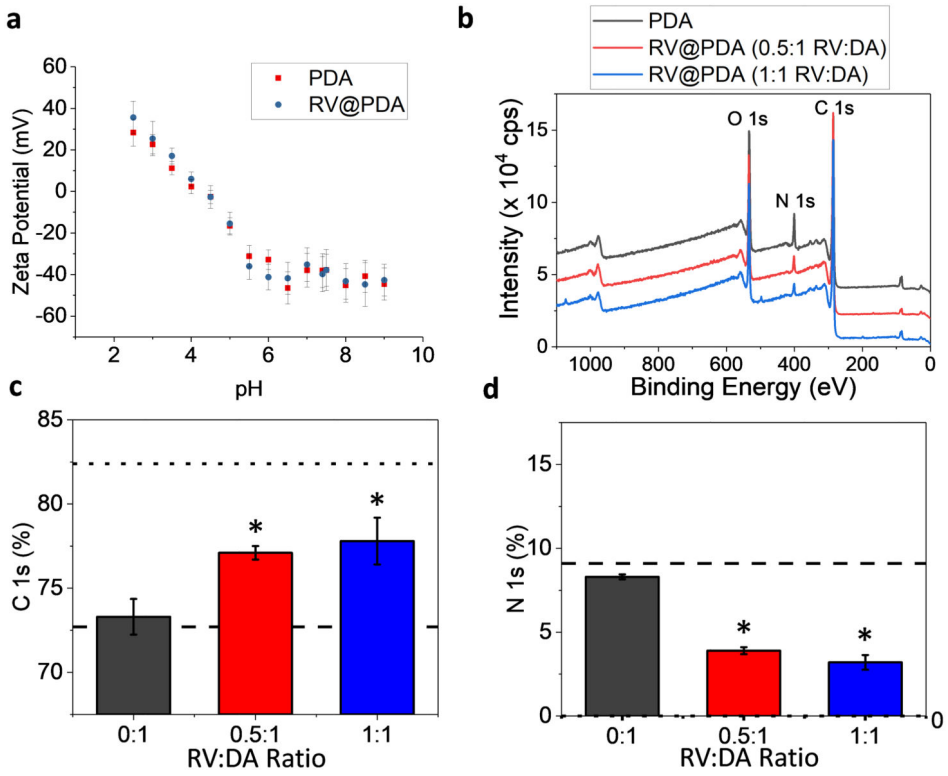


**Figure 3:**

Surface properties of PDA and RV@PDA evaluated by zeta potential and XPS. (**a**) Zeta potential vs. pH of PDA and RV@PDA. (**b**) Representative XPS survey spectra of PDA and RV@PDA prepared with 0.5:1 RV:DA and 1:1 RV:DA with O 1s, C 1s, and N 1s peaks indicated. (**c**) at% C and (**d**) at% N derived from high resolution XPS scans of C 1s and N 1s scans relative to total C, N, and O content for PDA (0:1 RV:DA) and RV@PDA (0.5:1 RV:DA and 1:1 RV:DA). The theoretical at% C and at% N for DA are indicated by dashed lines and those of RV with dotted lines. Error bars indicate SD. *: $p < 0.01$ versus 0:1 control.

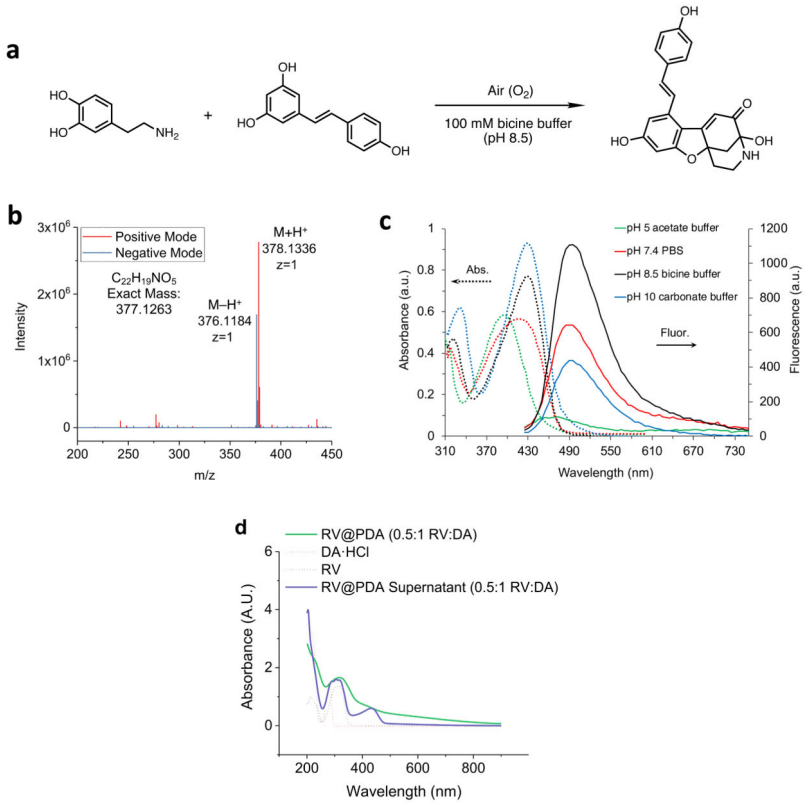


**Figure 4:**

Formation of a fluorescent azamonardine-type dopamine-resveratrol adduct. (**a**) Reaction of dopamine and resveratrol under alkaline conditions in air results in an azamonardine product. (**b**) High resolution positive and negative ion mode ESI mass spectrometry of dopamine-resveratrol adduct. (**c**) Absorbance and fluorescence emission spectra ($\lambda_{ex}$ = 390 nm) of pure dopamine-resveratrol adduct at 0.2 mg/mL in aqueous buffers (0.1 M) at various pH values. Spectrum in DI water was collected on the isolated trifluoroacetate salt of the adduct, obtained after purification by semi-preparative HPLC. (**d**) UV-Vis absorbance spectrum of pure RV@PDA (0.5:1 RV:DA) and the supernatant removed from the growth solution during centrifugation.

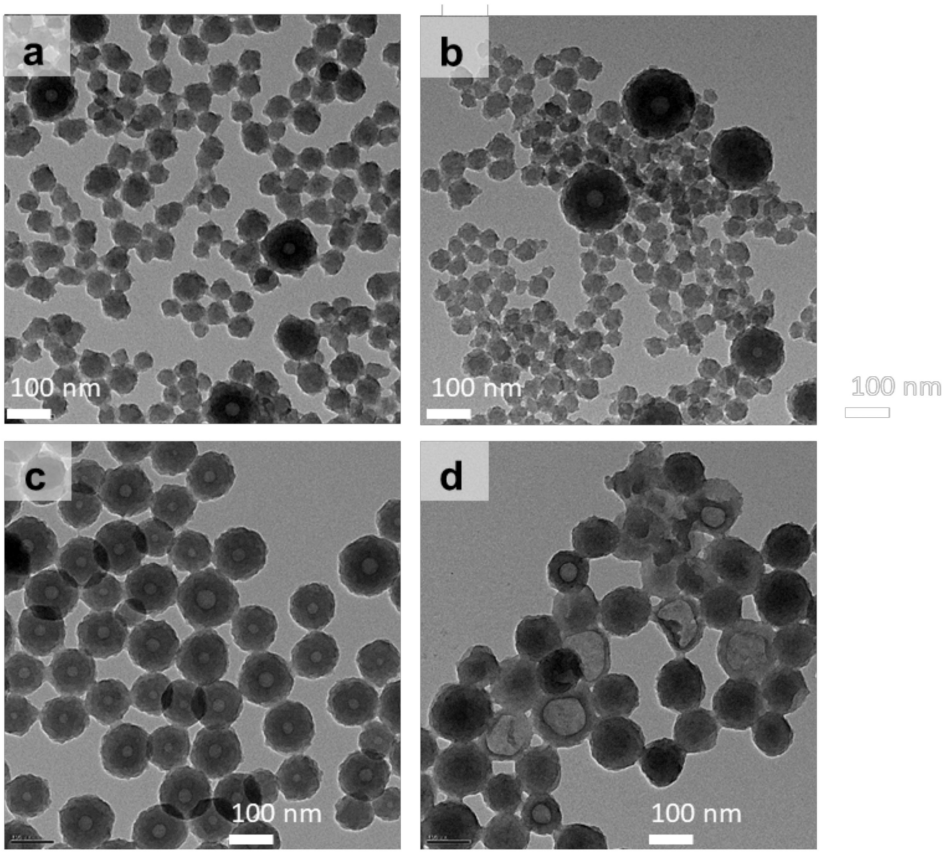


**Figure 5:**

TEM imaging of PDA and RV@PDA synthesized from solutions containing 0.25 mg/mL DA and 0:1, 0.1:1, 0.5:1, 1:1, and 2:1 RV:DA mass ratios. (**a**) PDA, (**b-d**) RV@PDA grown from solutions containing (**b**) 0.1:1 RV:DA, (**c**) 0.5:1 RV:DA, (**d**) 1:1 RV:DA.

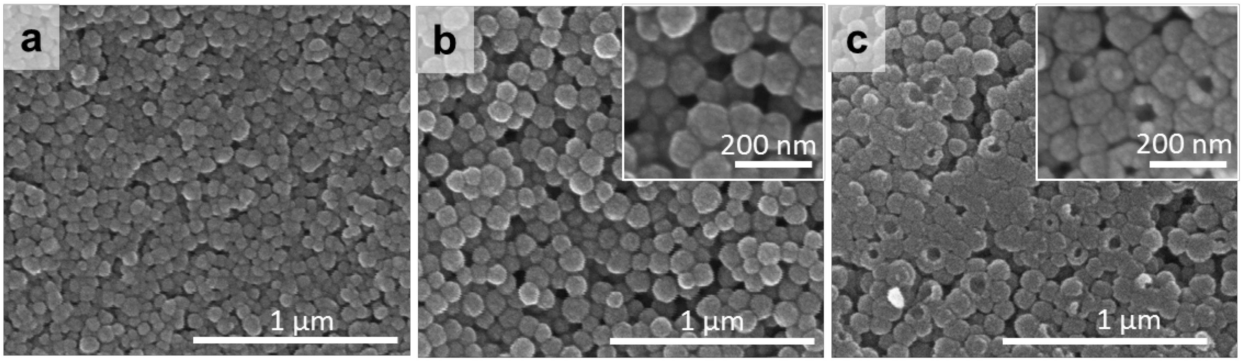


**Figure 6:**

SEM images of PDA and RV@PDA. (**a**) Native PDA. (**b-c**) RV@PDA (0.5:1 RV:DA) in native form (**b**) and following freeze-fracture (**c**).

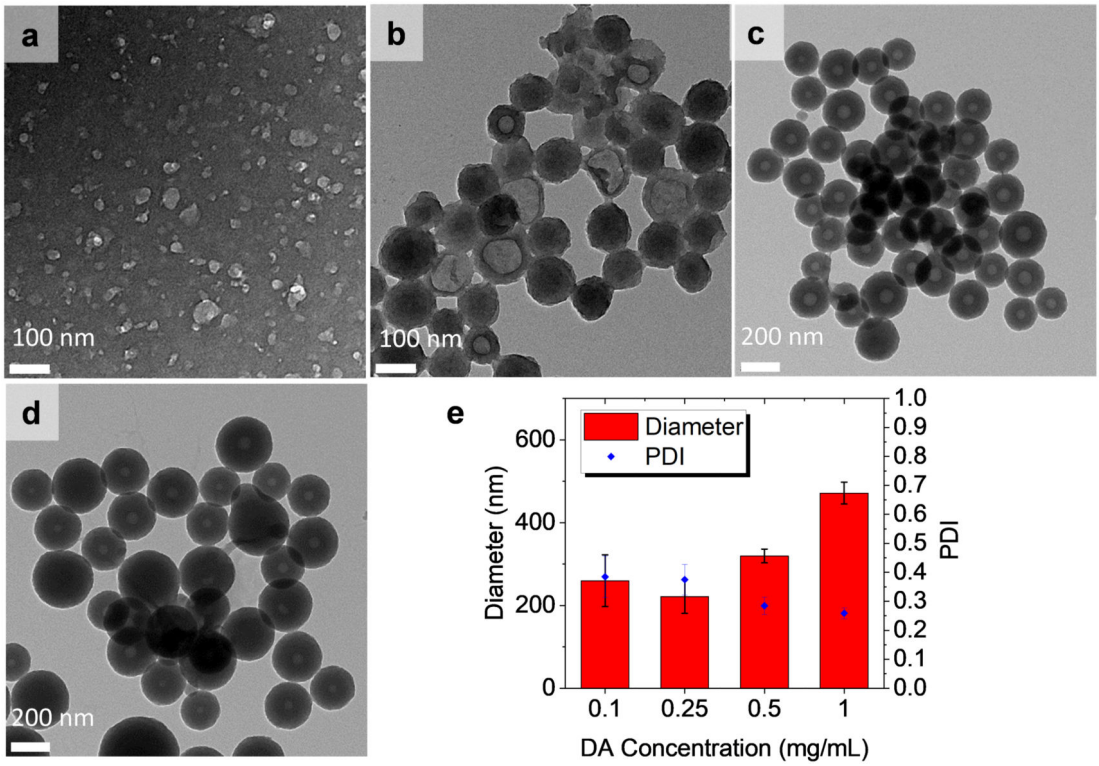


**Figure 7:**

Effect of DA concentration on RV@PDA grown in 0.25 mg/mL RV solution. (**a-d**) TEM images of RV@PDA grown with (**a**) 0.10, (**b**) 0.25, (**c**) 0.50, and (**d**) 1.00 mg/mL DA. TEM grids for (**b-e**) were prepared from purified nanostructures, and the TEM grid for (**a**) was prepared directly from growth solution after 24 h. (**e**) Hydrodynamic diameters and PDI of RV@PDA prepared with 0.10—1.00 mg/mL DA and 0.25 mg/mL RV measured by DLS. Error bars represent ± 1 SD of 3 independently prepared batches of RV@PDA. Data for DLS obtained from RV@PDA purified via centrifugation for 0.25 mg/mL—1.00 mg/mL DA and from growth solutions directly at 0.10 mg/mL DA after 24 h.

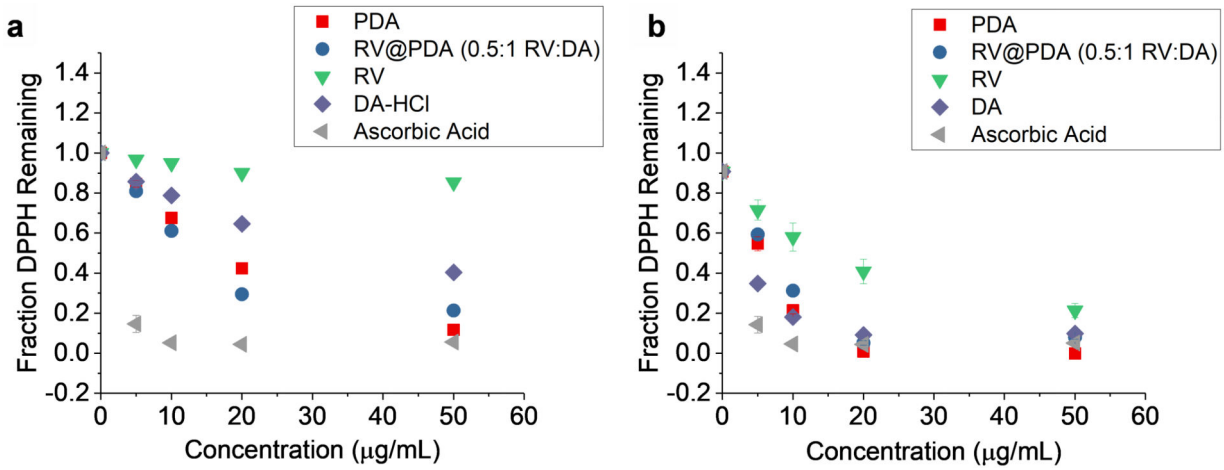


**Figure 8:**

Antioxidant activity of PDA NPs and RV@PDA NCs as evaluated by a DPPH assay. The fraction of DPPH radicals remaining after (**a**) 5 min and (**b**) 60 min is shown. DPPH scavenging for NPs is compared with free RV, DA, or ascorbic acid. Error bars indicate standard deviations.